Proceedings of the 11th ICPMG 2026
11th International Conference on Physical Modelling in Geotechnics
8-12 June 2026, Zurich, Switzerland

A centrifuge study on the dimensionless factor for drainage around large-diameter offshore monopiles

R. Fleminger, O. Adamidis*, C.M. Martin
University of Oxford, Oxford, UK

A. Agalianos, L. Jones, I. Anastasopoulos
ETH Zurich, Zurich, Switzerland

P. Peralta, N.C. Santos
Fugro NV, Leidschendam, Netherlands

orestis.adamidis@eng.ox.ac.uk

ABSTRACT: Offshore monopile foundations are increasing in size, to support ever-bigger wind turbines. Current monopile diameters are of the order of 10 m, with further increases planned. The assumption of a fully drained cyclic response for sand around monopiles, while sufficiently accurate for the small diameters used in the past, becomes unreliable for the large diameters used today (>10 m), as the longer drainage path around the monopile's circumference decreases the sand's capacity to fully drain within a load cycle. Designing such systems while accounting for partial drainage effects is the subject of ongoing research. An essential step in design will be the classification of the expected level of drainage, based on the properties of the monopile and the surrounding soil. In this work, a proposed dimensionless factor for drainage around large-diameter monopiles is examined using centrifuge experiments, performed at the beam centrifuge of ETH Zurich as part of the GEOLAB project. The proposed factor depends on the soil's bulk stiffness and hydraulic conductivity, and on the pile's dimensions. The results from three tests where the monopile was subjected to displacement-controlled loading are presented. Each test achieved the same value for the drainage factor through a different combination of loading frequency, pile diameter, and viscosity-adjusted hydraulic conductivity. The drainage response as represented by excess pore water pressures at homologous points of the different models is shown to be remarkably consistent across experiments, verifying the validity of the proposed dimensionless factor.

1 INTRODUCTION

The current trend in offshore wind turbine (OWT) development is toward wind farms comprising larger turbines, resulting in monopile foundations that frequently exceed 10 m in diameter. Existing research on monopiles with low slenderness ratios ($L/D \approx$ 3–6) has been extensive; however, for monopiles installed in sandy soils, much of this work is based on laboratory-scale model tests, element tests, or field scale tests conducted under fully drained conditions. Such assumptions may not be representative of in situ behaviour. For large-diameter monopiles, it is anticipated that fully drained conditions are unlikely to prevail, with the soil response being partially drained instead. The influence of monopile diameter on drainage behaviour has been proposed to be captured by the dimensionless parameter $MkT/\gamma_w D^2$ (Klinkvort *et al.*, 2018), where M is the constrained soil stiffness at a characteristic depth, k is the hydraulic conductivity, T is the loading period, and γ_w is the unit weight of water. The implication of this dimensionless drainage scaling factor is of reduced drainage with increased monopile diameter. A limited number of recent experimental (Zhu *et al.*, 2021; Takahashi *et al.*, 2022) and numerical (Jostad *et al.*, 2019; Kementzetzidis *et al.*, 2019; Chaloulos *et al.*, 2024) investigations have observed reduced drainage with increasing diameter. However, further work is required to validate the hypothesised factor as appropriate to characterise the drainage response.

The data from three centrifuge tests are included herein, each test with a different combination of D, k, and T but all designed to yield the same dimensionless factor $KkT/\gamma_w D^2$, with K being the bulk modulus. While the bulk modulus was selected as more appropriate for the factor controlling drainage around a monopile, the conclusions drawn would remain unaltered if the constrained modulus M were used, since all models were prepared using the same sand and the same air pluviation technique.

The tests presented here were performed on the beam centrifuge of the Geotechnical Centrifuge Centre (GCC) in ETH Zurich, as part of GEOLAB: project DROMOS (Adamidis, 2025).

2 METHOD

The soil deposit consisted of Congleton sand, pluviated through a curtain raining system to a target density of D_r = 80% (e = 0.58), in cylindrical strongboxes of 0.75m x 0.75m (diameter x height). The model monopiles were wished-in-place, to allow the installation of pile mounted sensors. An acceleration of 50g was targeted at 1/3rd of the monopile embedment depth. The models were saturated with methyl-cellulose solutions (Adamidis, 2015), prepared to the target viscosity of each test.

2.1 Monopile

The model monopiles were instrumented with accelerometers, pore pressure transducers (PPTs), and strain gauges; additionally, PPTs were installed in the soil. Instrument locations were defined relative to the monopile diameter to maintain consistency across tests. Further instruments included laser displacement transducers, a load cell, and an LVDT positioned on the soil surface (Figure 1).

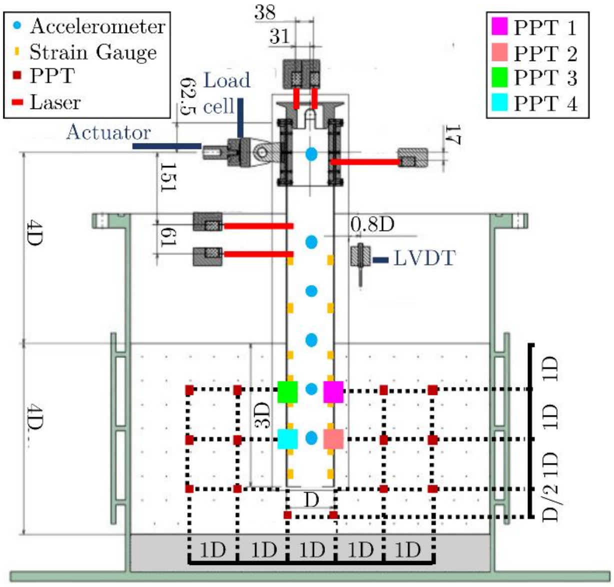

Figure 1. Instrumented monopile installed in a cylindrical strongbox. Model scale, dimensions in millimetres. Location of PPTs 1 to 4 labelled

To limit boundary effects, the maximum pile diameter was set so that the distance from the edge of the pile to the boundary of the strongbox would not fall below three pile diameters. In prototype scale, the monopile diameters tested were D_p = 4.15, and 5 m. Since the monopile diameters of interest for drainage exceeded 10 m, a double scaling procedure was implemented. The first scaling step was that imposed by centrifugal acceleration, as is typical in centrifuge testing. The second step aimed to match a reference dimensionless drainage factor, which corresponded to a large diameter monopile (≥10 m). For a test with a given combination of pile diameter and fluid viscosity, the prototype loading period was reduced, to achieve the same drainage factor, $KkT/\gamma_w D^2$, as that of the reference, larger monopile. The procedure for scaling the loading period is outlined in Equation 1, which assumes a square root dependence of bulk stiffness on depth. The resulting change in period is given in equation 2. The subscript '*ref*' corresponds to the reference, large monopile, and the subscript '*p*' corresponds to the prototype monopile.

$$\frac{K_{ref}\,k\,T_{ref}}{\gamma_w\,D_{ref}^2} = \frac{K_p\,k\,T_p}{\gamma_w\,D_p^2} = \frac{K_{ref}\sqrt{\frac{D_p}{D_{ref}}}\,k\,T_p}{\gamma_w\,D_p^2} \tag{1}$$

$$T_p = T_{ref}\left(\frac{D_p}{D_{ref}}\right)^{3/2} \tag{2}$$

Further, the structural properties of the monopile were scaled using the flexural response factor E_pI_p/E_sD^4 proposed by Klinkvort *et al.* (2018), where E_pI_p is the flexural rigidity of the pile and E_s is the Young's modulus of the soil. A D = 10m, steel (E = 210 GPa) reference monopile was selected, with the prototype and model monopiles matching its flexural response factor. Aluminium (E = 69 GPa) was used for the model monopile, to increase thickness and improve workability. The properties of the D_p = 4.15 m monopile are summarised in Table 2-1.

Table 2-1. Monopile properties

Parameter	Model	Prototype	Reference
Acceleration (g)	50	1	1
Diameter (m)	0.083	4.15	10
Emb. length (m)	0.249	12.45	30
Eccentricity (m)	0.332	16.6	40
Thickness (m)	0.0016	0.080	0.098
E (GPa)	69	69	210
EI_y (Nm^2)	2.33×10^4	1.46×10^{11}	7.85×10^{12}
Period T (s)	0.036	1.8	6.8

2.2 Testing details

The test results included in this paper form a subset of a larger experimental campaign conducted at the Geotechnical Centrifuge Centre (GCC) of ETH Zurich, as part of the GEOLAB project. Data from three tests of that campaign are presented here (T3, T4, and T5), focusing on the first loading event out of a sequence of loading events. Consequently, the data discussed here are not subject to any prior loading history, which could significantly influence the system response (Fleminger et al., 2025). Each of the presented events was applied as a displacement-controlled time history at the actuator level, with cyclic amplitude $y_a = 0.03D$, around a midpoint of $y_a = 0.015D$. Test details are given in Table 2-. The reference diameter D_{ref} is that for which the dimensionless drainage factor was calculated.

All loading events presented here share the same reference diameter (D_{ref} = 10 m) and loading period (T_{ref} = 6.8 s); hence, the same dimensionless drainage factor. However, the experimental configuration of each test differs. In test T3, the monopile had a prototype diameter of D_p = 4.15 m and the soil was saturated using a pore fluid of 50 cSt viscosity. Test T4 employed a monopile with a larger prototype diameter of D_p = 5.0 m, also saturated with a 50 cSt pore fluid. In contrast, test T5 used a monopile with D_p = 4.15 m but with a higher pore fluid viscosity of 66.5 cSt. All tests were conducted at a centrifugal acceleration of 50g. For each event, the pile diameter and the fluid viscosity where taken into account when calculating the loading period, T, chosen to match the dimensionless drainage of the reference monopile. The increased diameter in T4 and the increased viscosity in T5 both resulted in the same increase in prototype loading period as compared to T3.

While all loading events corresponded to the same drainage factor, the number of loading cycles varied. The number of cycles was increased in subsequent tests (the testing sequence was T4, T3, T5), as our understanding of the system response improved, with the aim of reaching a steady-state response by the end of the first loading event. The term steady-state within the context of this paper refers to approximate repetition of system load-displacement loops and in-soil pore water pressure cycles. Despite the different number of cycles between tests, reliable conclusions could be drawn, as discussed in the following section.

Table 2-2 Test details, including reference diameter

Test event	y_a/D	Cycles	D_p (m)	μ (cSt)	T_p (s)	D_{ref} (m)
T3_1	0.03	400	4.15	50	1.82	10
T4_1	0.03	200	5	50	2.44	10
T5_1	0.03	1000	4.15	66.5	2.44	10

3 RESULTS AND DISCUSSION

All loading events presented herein correspond to the same reference diameter, D_{ref} = 10 m, and reference loading period, T_{ref} = 6.8 s, and thus the same dimensionless factor for drainage. If this hypothesised drainage factor is valid, then the recorded drainage response at homologous points around the monopiles should match for all events, irrespective of the test-specific combination of pile diameter, hydraulic conductivity, and loading frequency.

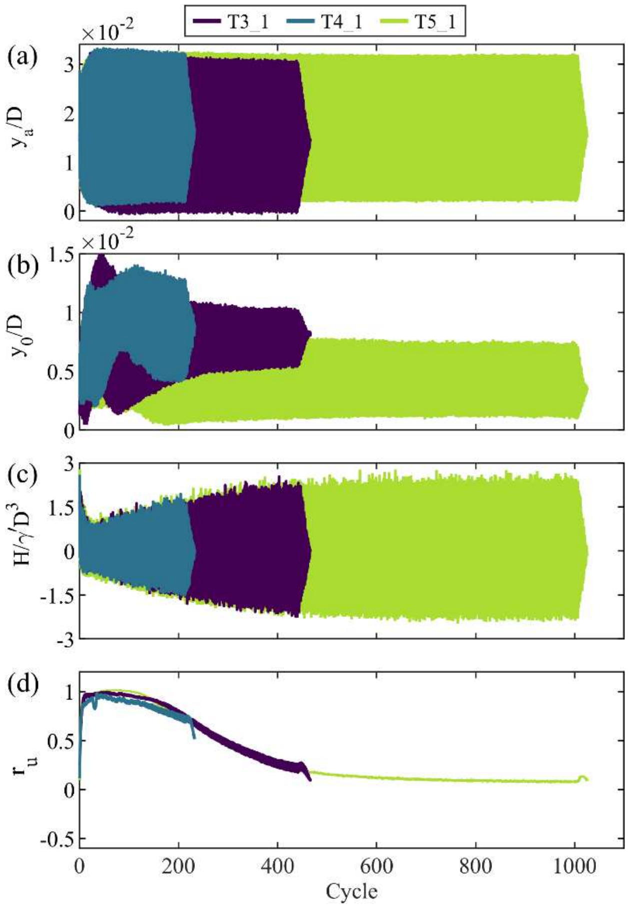

Figure 2. Normalised results of T3_1, T4_1, and T5_1 showing: (a) actuator displacement y_a/D, (b) mudline displacement y_0/D, (c) mudline load $H/\gamma'D^3$, (d) moving mean of r_u at PPT1 (location shown in Figure 1)

Figure 2 presents the evolution of the normalised actuator displacement y_a/D, the normalised pile head displacement y_0/D, the normalised horizontal load $H/\gamma'D^3$, with γ' the buoyant unit weight of the soil, and the moving mean of excess pore water pressure ratio (r_u), defined as the ratio of excess pore water pressure over the initial vertical effective stress. The plots are presented versus cycle number in the abscissa, to reconcile the different loading period between events T3_1, T4_1, and T5_1.

All events involved imposed displacement at the actuator level. Expectedly, the normalised actuator displacement y_a/D plots are consistent between the three tests, replicating the requested harmonic oscillations between $y_a = 0D$ and $y_a = 0.03D$. The amplitude of oscillation was gradually increased over the first cycles and gradually decreased over the last cycles through a ramp functions.

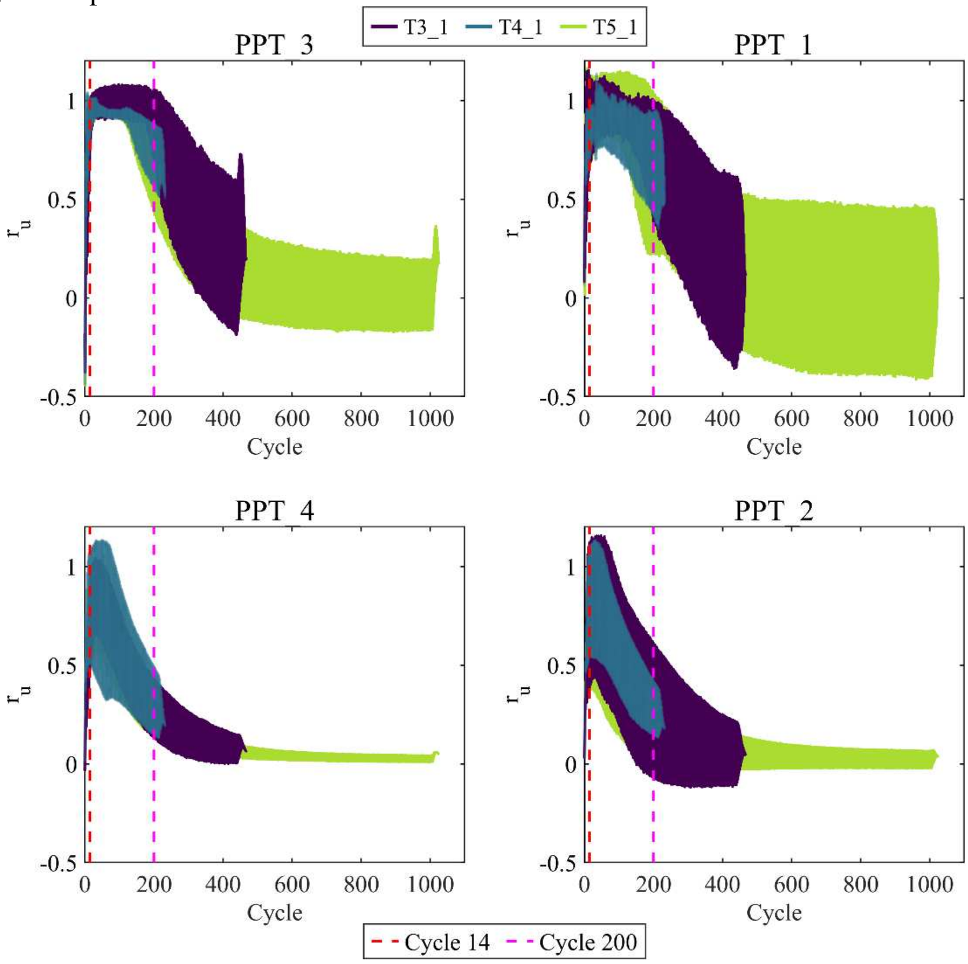

Figure 3. Full excess pore pressure response (r_u) at PPT1 during tests T3_1, T4_1, and T5_1. Overlaid are key cycles at which an excess pore pressure distribution is presented in Figure 4.

Excess pore water pressures increased rapidly over the first few cycles of loading, as shown in Figure 2d, which depicts the moving mean of the excess pore pressure ratio r_u for PPT1, at the interface of the pile and the soil, $1D$ below the mudline (see Figure 1). The curves of Figure 2d depict the average of a moving window equivalent to two loading cycles, to eliminate in-cycle pore pressure oscillation. The values of r_u quickly reached unity, implying liquefaction in the vicinity of the pile. This accumulation was discussed by Fleminger et al. (2025), where results from T3 were presented in more detail. While recorded in these experiments, initial liquefaction was deemed unrealistic for real monopiles. It was attributed to the collapsible fabric produced during model preparation via air-pluviation and the shadowing effects around the wished-in-place monopile, which resulted in up to 10% local reduction in relative density. Such dramatic accumulation of pore water pressure was not recorded in subsequent loading events, once the soil had been 'conditioned' by the initial loading.

Following the high levels of r_u, which were maintained for the first 100 cycles, excess pore pressures started to dissipate. In event T5_1, which included 1000 cycles, a steady-state was eventually reached, with pore water pressure dropping to an average value of $r_u \approx 0$. Event T4_1 with 400 cycles approached a steady state. Event T3_1, which included 200 cycles, did not reach a steady state.

The evolution of normalised horizontal load at the mudline (Figure 2c) was consistent across tests and can be interpreted based on the evolution of excess pore water pressure (Figure 2d). Initial liquefaction and the resulting reduction in system stiffness led to a quick drop in the amplitude of the horizontal load required to produce the imposed displacement cycles at the actuator level. As excess pore water pressures dissipated and the system stiffness was gradually recovered, the amplitude of the horizontal load required to produce the specified actuator-level displacement cycle increased. Approach to a load cycle steady state mirrored the approach to an excess pore water pressure steady state.

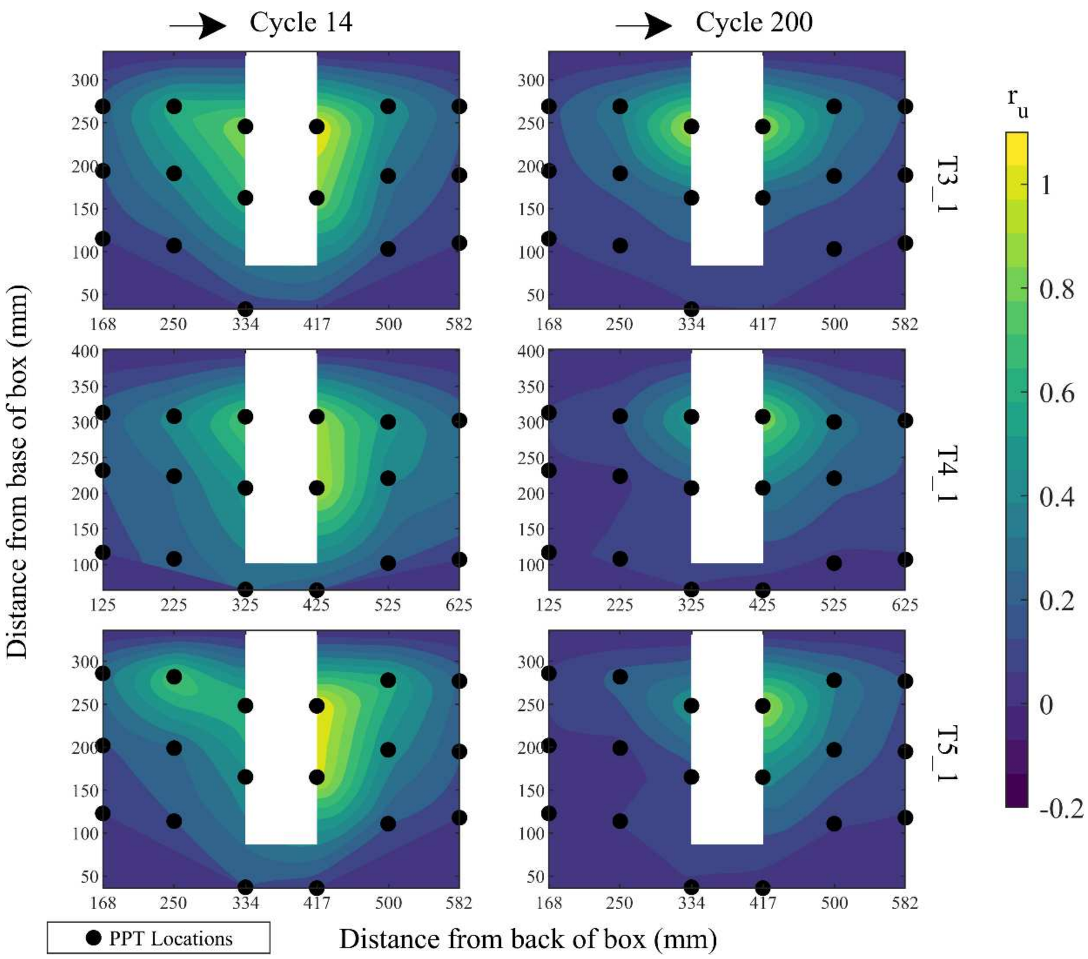

Figure 4. Contour plots of excess pore pressure, r_u, during T3_1, T4_1, and T5_1 at cycles 14 and 200.

The greatest differences between tests were recorded for normalised mudline displacement y_0/D (Figure 2b). All tests displayed an initial increase in both cyclic amplitude and cycle-average of mudline displacement, while the moving mean of excess pore water pressure ratio in Figure 2d held values close to unity. As excess pore water pressures started dissipating, mudline displacement cycles reduced in amplitude but maintained their previously obtained average values. These values were comparable for T3_1 and T4_1, but lower for T5_1. The amplitude of normalised mudline displacement oscillations at 200 cycles, when T4_1 was stopped, was comparable between T4_1 and T5_1 and slightly smaller for T3_1. Considered along with the actuator level displacement, y_a/D, the small differences in average mudline displacement between tests indicate small differences in the mean of mudline rotation.

Further discussion on the implications of the time histories of Figure 2 for the behaviour of a monopile can be found in Fleminger et al. (2025), which focuses on T3 and considers the effects of loading history on system response.

The aim of this paper is to examine the validity of the hypothesised dimensionless drainage factor $KkT/\gamma_w D^2$, which was kept the same between all three events presented. The moving mean of excess pore pressure ratio at the location of PPT1, shown in Figure 2d is highly consistent across all three events, both regarding the rate and magnitude of pore pressure accumulation, as well as the rate of dissipation, despite differences in pile diameter, loading period, and pore fluid viscosity across the three tests. Figure 3 presents the full excess pore water pressure ratio time histories of all four PPTs located at the pile-soil interface, as shown in Figure 1. The results reveal that initial liquefaction was reached at all monitored locations around the instrumented pile. Dissipation at PPTs 2 and 4, 2D below the mudline started sooner than at the shallower PPTs 1 and 3, 1D below the mudline. While excess pore water pressures dissipated at all four PPTs, their cycle-average values were similar and the amplitude of their oscillation was comparable. However, due to the higher value of initial effective stress at the deeper locations, these trends were altered in the plots of Figure 3, where excess pore water pressure ratio r_u is depicted. Indeed, the dissipation of r_u happened faster at the deeper PPTs and the amplitude of oscillation was lower. Even when a steady state was reached for the cycle average excess pore pressure, large, in-cycle oscillations persisted. Importantly for the question of interest here, the presented time histories of excess pore water pressure ratio were very similar at all four locations and for all three tests, providing strong evidence for the validity of the hypothesised dimensionless drainage factor.

Two key cycles are indicated on Figure 3, for which contours of excess pore water pressure ratio are shown in Figure 4, along the cross section of each model. The first cycle is number 14, the cycle with the maximum excess pore water pressure recorded at PPT1 during event T3_1, chosen to represent an instant at or near the triggering of initial liquefaction. The second cycle is number 200, selected as the final full loading cycle of event T4_1, before the amplitude of loading was ramped down, and representing a cycle well into the dissipation process. The contour plots presented in Figure 4 illustrate the spatial distribution of excess pore water pressure ratio at the instant of peak displacement amplitude for the selected cycles. The contours of cycle 14 reveal localised liquefaction at the pile-soil interface, with higher values of r_u developing at the front of the pile, in the direction of loading, and values of r_u quickly decreasing further away from the pile. The triggering of liquefaction would have been missed had the interface PPTs – a novelty of this experimental campaign – not been included. The contours of cycle 200 show that during the dissipation process, it was the shallow soil at the pile-soil interface that remained most vulnerable.

Some expected experimental variation between tests notwithstanding, the excess pore pressure ratio distributions demonstrate a remarkably consistent drainage response throughout the extent of the monitored soil cross section, for both time instances, across all three tests. These results provide further evidence on the validity of the selected dimensionless drainage factor as appropriate to characterise drainage throughout the soil deposit surrounding the monopile.

4 CONCLUSIONS

The results included in this paper provide strong evidence in support of the dimensionless factor $KkT/\gamma_w D^2$ as appropriate to characterise the drainage response around a monopile. Data from three centrifuge tests are presented, in all of which a monopile was wished-in-place in a uniform deposit of dense Congleton sand and subjected to a specified normalised displacement time history, applied at the same eccentricity through a hydraulic actuator. Each test had a unique combination of pile diameter and pore fluid viscosity (thus prototype hydraulic conductivity). Nevertheless, the loading period was calculated in each test so that the same dimensionless drainage factor could be obtained, equal to that of a reference, 10 m diameter monopile, loaded cyclically with a period of 6.8 s. Results from only the first loading events were considered, to allow similar initial conditions. Remarkable agreement was obtained between tests for the pore water pressure response, throughout the monitored area of the soil. Both the average pore water pressure accumulation and dissipation, as well as the in-cycle oscillation were consistent, supporting the validity of the selected dimensionless drainage factor. Additionally, the results justify the performed scaling of the loading period to capture the drainage response around monopiles of larger diameter than was practicable to test without introducing significant boundary effects. While an apparent implication is that the sand around a 10 m diameter pile could be susceptible to significant excess pore water pressure accumulation, it is believed that this aspect of response, only present in the first loading event, was an artefact caused by the initial sand fabric and by shadowing effects around the wished-in-place pile. Finally, it should be noted that the presented campaign did not investigate the influence of embedment depth, which was kept at a value of *L*/*D* = 3 for all tests.

ACKNOWLEDGEMENTS

This project was part of the DRainage around Offshore MOnopiles during Storms (DROMOS) project, funded by GEOLAB (EU H2020 grant 101006512). The authors are grateful for the financial support. Gratitude is also extended to the technical staff of the ETH Zurich Geotechnical Centrifuge Centre – Ralf Herzog, Markus Iten, Jürg Giger, and Sandro Barbieri – for their invaluable support.

REFERENCES

Adamidis, O. and Madabhushi, G. S. P. (2015) ‘Use of viscous pore fluids in dynamic centrifuge modelling’, *International Journal of Physical Modelling in Geotechnics*, 15(3), pp. 141–149. doi: 10.1680/ijpmg.14.00022.

Adamidis, O. (2025) GEOLAB - Transnational Access Project DROMOS - DRainage around Offshore MOnopiles during Storms. Dataset, doi: 10.5281/zenodo.15426077

Chaloulos, Y. K. *et al.* (2024) ‘Fully-Coupled cyclic time-history analyses of monopile foundations in sand’, *Ocean Engineering*, 298, p. 116691. doi: 10.1016/J.OCEANENG.2024.116691.

Fleminger, R., Adamidis, O., Martin, C. M., Ryan, G. V., Agalianos, A., Jones, L., Anastasopoulos, I., Peralta, P., Santos, N.C.. Experimental investigation of the drainage response around a large-diameter monopile. *5th International Symposium for Frontiers in Offshore Geotechnics* (ISFOG), Nantes, 2025.

Jostad, H. P. *et al.* (2019) 'Evaluation of soil models for improved design of offshore wind turbine foundations in dense sand', *Geotechnique*, 70(8), pp. 682–699. doi: 10.1680/JGEOT.19.TI.034.

Kementzetzidis, E. *et al.* (2019) 'Geotechnical aspects of offshore wind turbine dynamics from 3D non-linear soil-structure simulations', *Soil Dynamics and Earthquake Engineering*, 120, pp. 181–199. doi: 10.1016/J.SOILDYN.2019.01.037.

Klinkvort, R. T. *et al.* (2018) 'A review of modelling effects in centrifuge monopile testing in sand', *Physical Modelling in Geotechnics*, 1(July), pp. 719–724. doi: 10.1201/9780429438660-108.

Takahashi, A. *et al.* (2022) 'Centrifuge model tests on large-diameter monopiles in dense sand subjected to two-way lateral cyclic loading in short-term', *Soils and Foundations*, 62(3), p. 101148. doi: 10.1016/j.sandf.2022.101148.

Zhu, B. *et al.* (2021) 'Centrifuge Modeling of Monotonic and Cyclic Lateral Behavior of Monopiles in Sand', *Journal of Geotechnical and Geoenvironmental Engineering*, 147(8), p. 04021058. doi: 10.1061/(asce)gt.1943-5606.0002566.